Available online at www.CivileJournal.org

Civil Engineering Journal

(E-ISSN: 2476-3055; ISSN: 2676-6957)

Vol. 12, No. 06, June, 2026

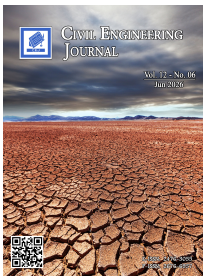

Optimization of Deflector–Groove Aerator Location for Cavitation Mitigation on Spillway Chutes: A CFD-Based Investigation

Marojahan Lumban Gaol [1*], Pitojo Tri Juwono [1], Very Dermawan [1], Dian Sisinggih [1], Lily M. Limantara [1*]

[1] *Department of Water Resources Engineering, Faculty of Engineering, University of Brawijaya, Malang, Indonesia*.

Received 19 November 2025; Revised 21 May 2026; Accepted 24 May 2026; Published 01 June 2026

Abstract

Cavitation in high-velocity spillways is a critical issue in modern hydraulic design, particularly in channels with downward concave vertical curvature, which are vulnerable to negative pressure and jet reattachment. This study aims to evaluate the influence of aerator position, using a deflector-groove type, on flow characteristics, pressure distribution, entrained air mass, and the cavitation index in a multi-slope spillway through CFD-based numerical simulation. Five aerator configurations, labeled A to E, were analyzed under a design discharge of 1,154.3 m^3/s, using the SST k–ω turbulence model and mesh sizes ranging from 220 to 500 mm. Validation against physical data showed a high level of significance, with $R^2 > 0.9$, confirming the reliability of the numerical model used. The velocity distribution indicates that the aerator location significantly influences air-jet formation and air-cavity stability. The aerator positioned at the center of the concave section, Series A, produced the most stable flow pattern, controlled negative pressure, and an entrained air mass of 63 kg/s. In addition, the cavitation index value for Series A showed an average increase of up to 20% compared with the other configurations, indicating the effectiveness of this position in reducing cavitation potential. Based on the integrated results of pressure, aeration, and cavitation index, the Series A configuration is recommended as the optimal position for spillways with a downward concave vertical curve geometry. This finding reinforces the established aeration theory reported in previous studies and provides a practical contribution to the optimization of aerator design in complex spillways.

Keywords: Spillway Aerator; Deflector–Groove; Cavitation Index; CFD Simulation; Aeration Efficiency.

1. Introduction

Research on spillway aerators has grown rapidly over the past several decades in response to the increasing demand for mitigating cavitation risks caused by high flow velocities along spillway chutes. Cavitation occurs when local pressure drops below the vapor pressure of water, leading to vapor bubble formation and potentially severe damage to concrete surfaces [1-4]. The performance of spillway aerators is strongly influenced by chute geometry, flow discharge, atmospheric conditions, and the configuration of aeration elements. Gaskin et al. [5], Aydin [6], and Wang et al. [7] demonstrated that air demand increases with increasing chute slope and Froude number, highlighting the critical role of aeration in stabilizing pressure under supercritical flow conditions.

The development of experimental and numerical methods over the last two decades has substantially strengthened the understanding of aeration mechanisms in spillways. Physical model studies by Wu et al. [8] showed that minimum

* Corresponding author: lumbangaolmarojahan@gmail.com; lilymont@ub.ac.id

https://doi.org/10.28991/CEJ-2026-012-06-011

cavity pressure increases significantly with increasing channel slope. These findings were further extended by Ma and Wu [9], and Wu et al. [10] through experimental and numerical turbulence analyses, confirming that hydraulic parameters such as flow velocity, water depth, and jet trajectory strongly influence cavity stability and flow regime transitions. Furthermore, Qian et al. [11] and Wang et al. [7] identified that the interaction between jet impingement, re-attachment zones, filling water, and atmospheric pressure variations is a primary source of local pressure fluctuations that may trigger cavitation in high-velocity spillways.

Studies on natural self-aeration have also provided important contributions to modern aerator design. Wei et al. [12] demonstrated that increasing initial velocity and flow depth accelerates air diffusion in supercritical flows, showing that turbulence intensity—rather than Froude number alone—governs the development of self-aeration. These findings were reinforced by Bai et al. [13], Liu et al. [14], and Liu et al. [15], who showed that bubble dynamics, turbulence dissipation rate, and scale effects play a critical role in controlling air concentration distribution and near-bed protection against cavitation.

Deflector–groove aerators remain among the most widely applied solutions due to their ability to generate stable jets and sustained air cavities beneath the main flow layer [5, 6, 9]. Numerous studies have demonstrated that deflector and groove geometries directly affect air intake rate, cavity length, pressure fluctuations, fin formation, and air concentration diffusion along the chute [8, 10, 11, 16]. Su et al. [17] reported that trapezoidal intermittent deflectors are effective in improving aeration efficiency on mildly sloping spillways with low Froude numbers, while Yang et al. [18] and Li et al. [19] emphasized that ventilation layout and predictive models for air demand are essential for maintaining aeration performance, particularly for wide spillways and complex geometries.

Beyond aerator geometry, the geometry of the chute bed itself plays a critical role in pressure stability and cavitation susceptibility. Felder & Chanson [2], Pfister & Chanson [3], and Salehi et al. [4] showed that flows over spillways with concave vertical curvature, bends, or geometric transitions are particularly vulnerable to extreme pressure gradients, jet impingement, and cavitation inception. Similar observations were reported by Aydin et al. [20] and Bagherzadeh et al. [21], who demonstrated that high-velocity zones and curvature transitions can be reliably identified as cavitation-prone regions using CFD and data-driven approaches, yet still require effective aeration as a physical mitigation measure.

With advances in computational capability, *Computational Fluid Dynamics* (CFD) has become a powerful tool for systematically optimizing aerator design. Dong et al. [22] developed a parabolic ramp-type aerator for mildly sloping chutes and demonstrated improved pressure distribution stability. Yang et al. [18], Ali et al. [23], and Safiloo et al. [24] investigated the effects of aerator type, ventilation layout, spacing, and positioning, showing that multi-aerator configurations or combined ramp–offset systems significantly enhance air-layer continuity and cavitation index. Meanwhile, Kalateh & Aminvash [25] explicitly demonstrated that aerator location, rather than aerator presence alone, governs pressure reduction effectiveness in complex spillway systems.

Despite extensive experimental, numerical, and data-driven evidence confirming that aerator geometry, type, and configuration influence aeration efficiency [18, 19, 24], most existing studies remain focused on single-slope chutes or simplified geometries. Systematic investigations addressing the influence of aerator location on multi-slope spillways—particularly those incorporating concave vertical curvature, low atmospheric pressure conditions, and scale-sensitive aeration processes—are still limited [3, 15, 26]. This gap represents an important challenge in modern spillway design for cavitation mitigation in high-energy hydraulic structures.

Cavitation risk in high-velocity multi-slope spillways is primarily governed by local pressure reduction, flow acceleration, and the stability of air–water interaction near the chute surface, particularly at concave vertical transitions. Aerators mitigate this risk by forming a deflected jet and a stable air cavity that entrains atmospheric air and promotes pressure recovery along the chute bed. Accordingly, aerator performance can be evaluated using key hydraulic and aeration indicators, including local pressure (p), flow velocity (V), cavitation index (σ), and aeration effectiveness quantified by air entrainment ratio (β). In complex spillway geometries, previous studies indicate that the longitudinal placement of an aerator relative to zones of flow acceleration and curvature plays a dominant role in controlling pressure recovery and the persistence of bottom aeration.

The present study is motivated by physical model observations at Tigadihaji Dam [27], which revealed localized negative pressures along a multi-slope chute with concave vertical curvature. To address this condition, a deflector–groove aerator with fixed geometric dimensions is applied at five different locations along the chute. A numerical approach based on the Volume of Fluid (VOF) method coupled with the SST k–ω turbulence model is employed to

evaluate the influence of aerator location on pressure distribution, flow velocity characteristics, and cavitation index. By isolating aerator location as the primary design variable, this study aims to identify an optimal placement strategy for cavitation mitigation in high-velocity multi-slope spillways. The findings are expected to contribute to practical design guidelines and to enhance the understanding of aeration mechanisms in high-energy hydraulic structures. The scope of the study is limited to a single deflector–groove aerator geometry, variations in aerator location within one multi-slope spillway configuration, and supercritical flow conditions analyzed using a two-phase numerical approach.

The remainder of this study is organized as follows. Section 2 material and method which describes the spillway geometry, aerator configurations, numerical model, and cavitation index formulation. Section 3 presents the results of pressure distribution, air entrainment, and cavitation index for different aerator locations, followed by a discussion of the optimal placement. Finally, Section 4 summarizes the main findings and conclusions of the study.

2. Material and Methods

2.1. Model of Spillway and Aerator

The Tigadihaji Dam is a 122 m high vertical-core rock-fill dam located on the Selabung River, South Sumatra, Indonesia. The dam is equipped with a side-channel spillway consisting of an 80 m wide crest, a 60.5 m wide transition channel, and a chute with a constant width of 35 m. The chute extends over a length of 769.7 m, comprises four segments with different bed slopes, and discharges into a stilling basin. The total spillway length from crest to stilling basin is approximately 992.7 m, with an overall energy head difference of 115.3 m.

A three-dimensional (3D) numerical model of the spillway was developed at full prototype scale (1:1) to represent the hydraulically critical portion of the chute, specifically chute segments 3 and 4 (Figure 1). These two segments have bed slopes of 1:35 and 1:1.5, respectively, and are connected by a concave vertical curve with a radius of 50 m and a curve length of 27.97 m.

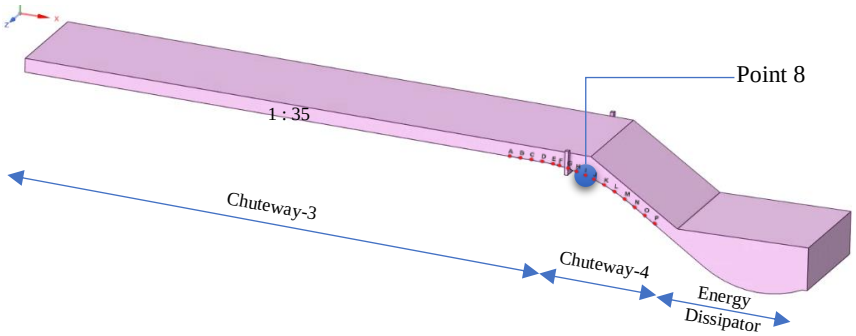

Figure 1. Model of 3D-Chuteway-3 to Energy Dissipator with Aerator at the Location of Point-8 and Measurement Points (A-P)

Previous physical model investigations conducted by the Indonesian Institution of Hydrology and Water Resources Geotechnics (2022) identified persistent negative pressures within the concave vertical curve, particularly at measurement point 8 (Figure 1). The minimum pressure recorded reached −5.25 mH_2O under high-discharge conditions (probable maximum flood discharge Q_{PMF}), as summarized in Table 1. To mitigate this risk, a deflector–groove type aerator (Figure 2) was incorporated into the model. The aerator includes sidewall air ducts that allow atmospheric air to be entrained through an air cavity formed beneath the deflected jet.

Table 1. Result of Piezometer Reading at Physical Model of Point-8

Discharge	Q_2	Q_{100}	Q_{1000}	Q_{PMF}
P (mH_2O)	-0.1	-1.15	-1.35	-5.25

Source: Indonesian Institution of Hydrology and Water Resources Geotechnics (Balai Hidrologi dan Geoteknik Keairan), 2022

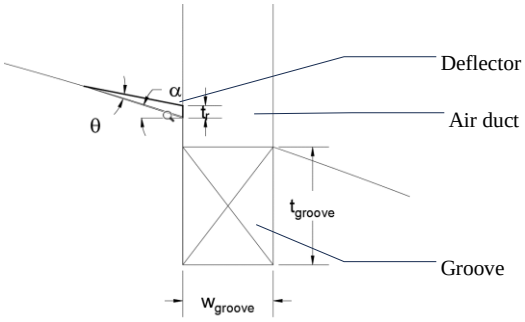

Figure 2. Geometry Schematic of Deflector and Groove Type-Aerator

Five aerator locations were investigated along the chute (Table 2); the positions were selected to systematically represent upstream, central, and downstream locations relative to the concave vertical curve, where physical model observations identified the most critical pressure reduction zone. Intermediate positions were evaluated in preliminary tests and showed similar trends, so the final five locations were chosen to capture the governing hydraulic behavior while keeping the parametric study efficient. All simulations employed an identical aerator geometry, allowing the effects of aerator placement to be evaluated independently of geometric variations. The design follows the concept proposed by Pfister & Chanson [3], with a deflector angle of 6.63°, a groove width of 1.0 m, a groove height of 1.3 m, and a total air-duct area of 1.3 m². The influence of aerator location was evaluated based on minimum pressure, cavitation index, and entrained air volume to identify the optimal placement within the concave vertical curve.

Table 2. Geometric Parameter and the Location of Deflector–Groove Type-Aerator

Series	Bed Slope α (°)	Distance of aerator from the initial point of model (m)	Height of deflector t_r (mm)	Angle-deflector θ (°)	Width of groove (m)	Height of groove (m)	Area of Air duct (m^2)
A	17.74	168.5	135	6.63	1.0	1.3	1.3
B	8.72	161.5	135	6.63	1.0	1.3	1.3
C	3.20	156.0	135	6.63	1.0	1.3	1.3
D	28.03	176.5	135	6.63	1.0	1.3	1.3
E	33.69	185.5	135	6.63	1.0	1.3	1.3

2.2. Numerical Setup

Numerical simulations were conducted to evaluate the influence of aerator location on pressure distribution, flow velocity, and cavitation potential along the spillway chute. At the inlet boundary, a discharge corresponding to the 1000-year return period flood (Q_{1000} = 1,154.3 m³/s) was prescribed with a water surface elevation of 1,462 m. The outlet boundary was defined as a free outflow at atmospheric pressure (101,325 Pa). The upper boundary of the computational domain was specified as a pressure outlet, allowing free air exchange with the atmosphere, while the lateral and bottom boundaries were treated as no-slip walls representing the spillway surfaces.

The simulations were performed using ANSYS Fluent with the Volume of Fluid (VOF) method to model the two-phase air–water flow and capture the free-surface interface. Turbulence was represented by the shear stress transport (SST) k–ω model, which is suitable for high-velocity flows with strong pressure gradients, flow separation, and jet–air interactions near aerator structures. All simulations were carried out under steady-state conditions. The computational mesh consisted of a hexahedral-dominant grid, with cell sizes ranging from 220 mm to 500 mm. Local mesh refinement was applied in the vicinity of the deflector, groove, and channel walls to improve the resolution of pressure gradients and air–water interactions. Convergence was achieved when the residuals of all governing equations dropped below 10^{-5} and the monitored hydraulic variables reached stable values.

Five simulation cases (Cases A–E) were analyzed, each representing a different aerator location within the concave vertical curve (Table 2). For each case, pressure distribution along the chute bed, jet velocity characteristics, and air entrainment beneath the jet were extracted for subsequent analysis. The validation of the numerical model is carried out by comparing the simulation result to the physical model data with a 1:1 scale that is developed by the Indonesian Institution of Hydrology and Water Resources Geotechnics (2022).

Figure 3 presents the workflow of the study, from problem identification and numerical model development to validation, cavitation risk assessment, and optimization of aerator location on a multi-slope spillway.

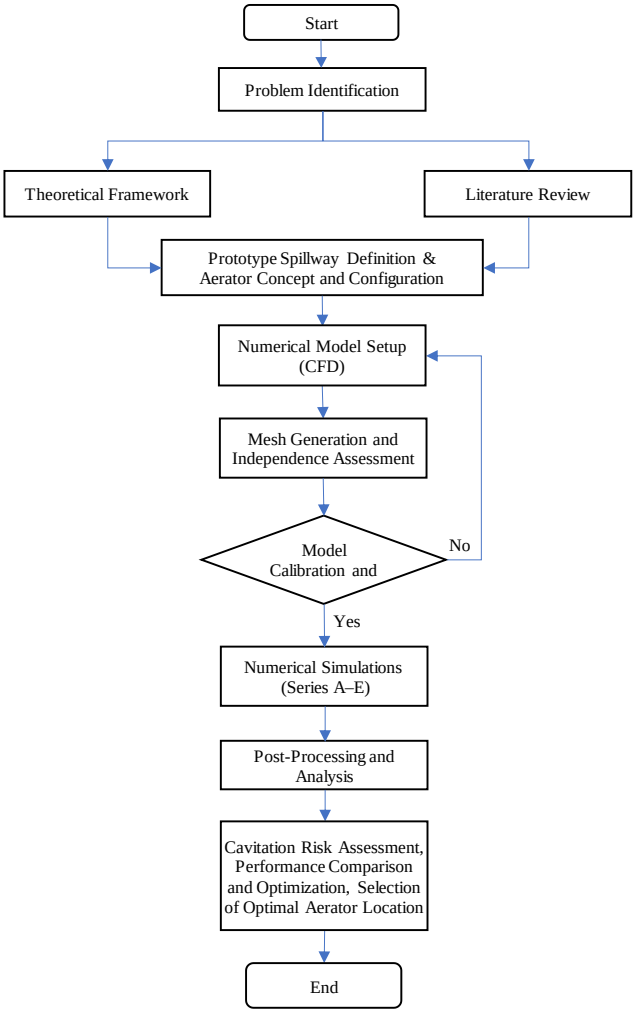

Figure 3. Flowchart of the research methodology

2.3. Cavitation Index

The cavitation index (σ) is used for evaluating the cavitation that happens along the spillway chute-way surface. This value is analysed based on the distribution of pressure as the numerical simulation result by using the formulation as follows:

$$\sigma = \frac{P_0 - P_v}{\rho v_0^2 / 2} \quad (1)$$

$$P_0 = P_a + P_g \quad (2)$$

where, P_0 is the ambient pressure (kPa); P_v is the water vapour pressure (kPa), ρ is the volume-mass of water (kg/m^3), P_a is the atmosphere pressure (101 kPa); and P_g is the local pressure (kPa).

The pressure and velocity values were extracted at observation points A to P, which are distributed along the spillway bed surface in the vicinity of the aerator. These data were used to determine the spatial distribution of the cavitation index (σ), which serves as the primary indicator for assessing cavitation risk at each location. The evaluation of cavitation risk was conducted by comparing the computed cavitation index with threshold criteria recommended by Falvey [28]. According to these criteria, flow conditions characterized by σ values greater than unity are generally regarded as safe and unlikely to induce cavitation damage. As σ decreases to the range of approximately 0.6–1.0, the likelihood of cavitation initiation remains low and is typically associated with light cavitation. Moderate cavitation effects may develop when σ falls between about 0.4 and 0.6, whereas a substantially higher cavitation risk is expected for σ values in the interval of 0.2–0.4. Values of σ below 0.2 indicate a severe cavitation condition with a high potential for significant structural damage.

In addition, the simulation result is verified by observing the correlation between the numerical pressure distribution and the physical model through the Root Mean Square Error (RMSE) and the determination coefficient (R^2). This validation makes sure that the CFD result can represent the phenomenon of real hydraulic with the accuracy level that can be accepted for the cavitation evaluation.

3. Results and Discussion

3.1. Model Calibration and Validation

3.1.1. Pressure Validation

The numerical model was calibrated and validated using prototype-scale physical model data of the Tigadihaji spillway, with particular attention to the hydraulically critical concave vertical curve between chute segments 3 and 4. Model calibration focused on selecting appropriate turbulence closure, free-surface treatment, and mesh refinement to accurately capture strong flow acceleration, jet formation, and pressure gradients in the aerated flow region. Sensitivity checks were conducted to ensure numerical stability and convergence of pressure fields in zones prone to cavitation.

Model validation was carried out by quantitatively comparing bed pressure measurements obtained from the physical model with corresponding numerical results at observation points 7–11 (Table 3), which are located within and downstream of the concave vertical curve where negative pressures were previously identified. Pressure was selected as the primary validation parameter, as it directly governs cavitation inception and represents the most relevant indicator for assessing aerator performance and cavitation risk.

Table 3. Physical model and CFD pressure (p) comparison at observation points 7–11 under different discharges

Point	p (mH_2O)							
	Q2		Q100		Q1000		QPMF	
	Physical	CFD	Physical	CFD	Physical	CFD	Physical	CFD
7	1	1.1	2.25	1.1	2.05	1.5	5	3.4
8	-0.1	0.08	-1.15	-0.3	-1.35	-0.31	-5.25	-3.1
9	-0.1	0.2	0.15	0.22	-0.4	0.5	1	1.02
10	1.15	1.07	4.9	3.1	3.8	3.8	24.5	27
11	-4.9	-3.9	-5.5	-4.1	-5.2	-4.7	-7.8	-8.2

Comparisons were performed for multiple discharge conditions (Q_2, Q_{100}, Q_{1000}, and Q_{PMF}). The results show that the numerical model successfully reproduces the spatial distribution and sign of pressure observed in the physical model. In particular, both numerical and experimental data consistently indicate negative pressures at Point 8 and Point 11, confirming these locations as the most critical zones for cavitation development. The maximum negative pressure was recorded at Point 8 under Q_{PMF} conditions, reaching −5.25 mH_2O in the physical model and −3.10 mH_2O in the numerical simulation, demonstrating that the CFD model captures the location and trend of extreme pressure reduction, albeit with a moderate underestimation of magnitude. Positive pressure zones at Points 7 and 10 were also well reproduced, indicating that the model accurately represents pressure recovery downstream of the aerator and transition zone.

The agreement between numerical and physical pressure data was evaluated using the coefficient of determination (R^2) and the root mean square error (RMSE) based on pressure values at Points 7–11 for all investigated discharges. The analysis yielded R^2 values exceeding 0.90, indicating a strong correlation between numerical predictions and experimental measurements, while RMSE values remained below 10%, confirming acceptable accuracy for engineering assessment. Examination of pointwise errors shows that the largest discrepancies occur in regions of intense aeration and jet impingement, where two-phase turbulence and scale effects inherently increase uncertainty in both measurements and numerical predictions. Nevertheless, the numerical model reliably reproduces the pressure minima and gradients governing cavitation risk.

3.1.2. Mesh Independence Assessment

A mesh-independence assessment was conducted using three computational meshes with approximately 2,320,485, 1,420,090, and 846,529 cells to ensure numerical stability of the results. The evaluation focused on bed pressure distributions at representative observation points D–I (Table 4) and on the entrained air mass flow rate at the aerator, both of which are critical for cavitation assessment. The pressure profiles obtained with the two finer meshes show very close agreement in both magnitude and spatial trend, including the location of pressure minima, whereas the coarser mesh exhibits noticeable deviations in regions of strong pressure gradients. A similar convergence trend is observed for aeration performance: the predicted air mass flow rates for the two finer meshes differ only slightly (45.25 kg/s and 42.99 kg/s), while the coarser mesh significantly underestimates air entrainment (0.25 kg/s). Based on the convergence of both pressure and air entrainment results, the mesh with 1,420,090 cells was selected for all subsequent simulations, providing mesh-independent predictions with reasonable computational efficiency.

Table 4. Mesh-independence assessment based on bed pressure at observation points D–I

Point	P (Pa) for different mesh resolutions		
	2320485	**1420090**	**846529**
D	4086	4434	4248
E	11890	11770	10660
F	6952	5759	1078
G	-1227	-1691	-4406
H	-1118	-1291	1984
I	-1126	-1026	2195

3.2. Characteristics of Flow

3.2.1. Effect of Aerator Position to the Flow Separation and Air Cavity

Numerical simulations were conducted for a constant discharge of 1,154.3 m³/s to examine the influence of aerator position on flow separation, jet behavior, and air cavity formation along the multi-slope chute. Figure 4 illustrates the water–air volume fraction distributions for the five aerator configurations (Series A–E), revealing distinct flow regimes governed primarily by the longitudinal location of the aerator relative to the concave vertical curve.

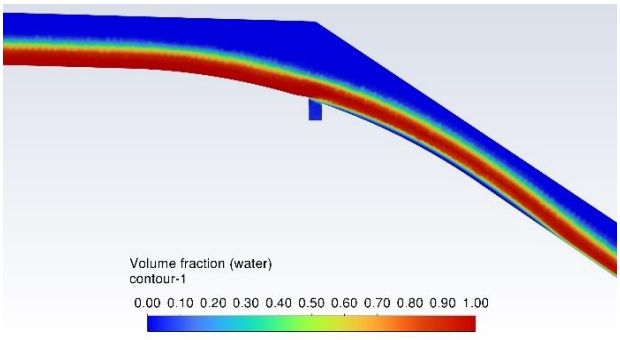

(a) Series-A

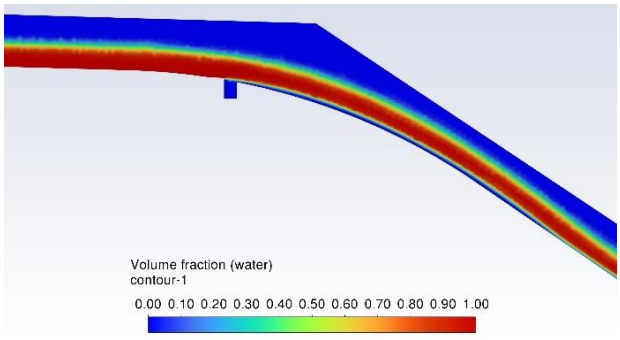

(b) Series-B

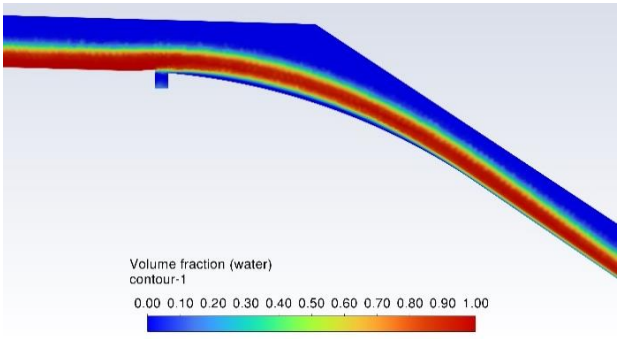

(c) Series-C

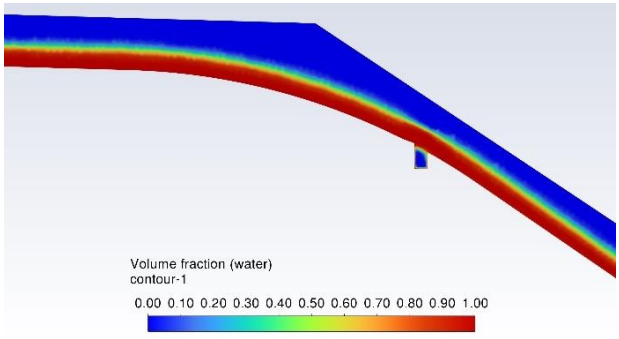

(d) Series-D

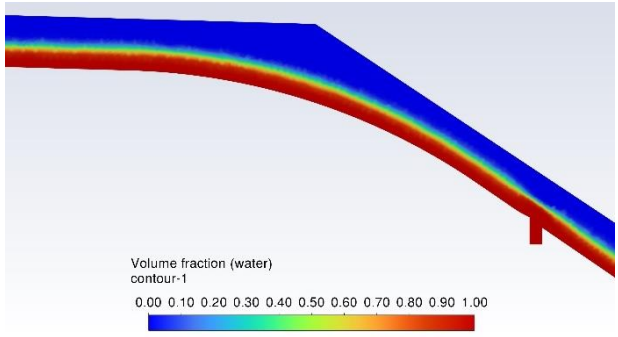

(e) Series-E

Figure 4. Volume Fraction of Water-Air at Chute-way

For Series A–C (Figures 3-a and 3-c), where the aerator is positioned upstream of or near the slope transition, the flow separates from the chute bed immediately downstream of the deflector, forming a free jet and a partially developed air cavity. Zones of elevated air content near the bed indicate cavity initiation beneath the jet, while high water volume fractions above the cavity represent the main flow layer. This flow pattern corresponds to partial aeration with an unstable or limited cavity length, consistent with observations reported for deflector–groove and offset aerators operating in moderate acceleration zones [3, 6, 14]. Such configurations are known to induce intermittent re-attachment of the jet, which may lead to local pressure fluctuations downstream of the cavity [8, 9].

In contrast, Series D and E (Figures 3-d and 3-e), where the aerator is placed further downstream on steeper chute segments, exhibit rapid flow re-attachment with no sustained air cavity formation. The water–air mixture remains dominated by high water volume fractions along the bed, indicating that the jet throw angle and local pressure reduction are insufficient to maintain a free jet and stable cavity. Similar attached-flow behavior has been reported in numerical and experimental studies when aerators are located too far downstream of peak acceleration zones, resulting in reduced cavity stability despite substantial air supply [22, 24].

Comparatively, Series A–C represent a separated-flow regime with partial cavity formation, whereas Series D–E correspond to an attached-flow regime with limited effective aeration. This transition highlights that increasing the downstream distance of the aerator promotes flow stability but reduces the ability to sustain an air cavity beneath the jet. Previous studies on high-head and multi-aerator spillways similarly emphasize that aerator effectiveness depends not only on air supply capacity, but also on its position relative to zones of rapid pressure reduction and curvature-induced acceleration [23, 25].

Overall, the results demonstrate that aerator location governs the balance between flow separation and re-attachment. An effective configuration requires placement sufficiently upstream to trigger cavity formation and air entrainment, while avoiding excessively long or unstable cavities that may amplify pressure oscillations. This finding is fully consistent with established theoretical and experimental frameworks for aerator design on high-velocity spillways with complex geometries [3, 20, 26].

3.2.2. Distribution of Pressure

The pressure distribution along the chute bed provides a direct indication of cavitation risk and reflects the interaction between flow acceleration, aerator-induced jet behavior, and channel geometry. Figure 5 presents the spatial distribution of static pressure for all aerator configurations under the design discharge condition (Q = 1,154.3 m³/s), while Figure 6 summarizes the corresponding pressure measurements at discrete observation points along the chute for Series A–E.

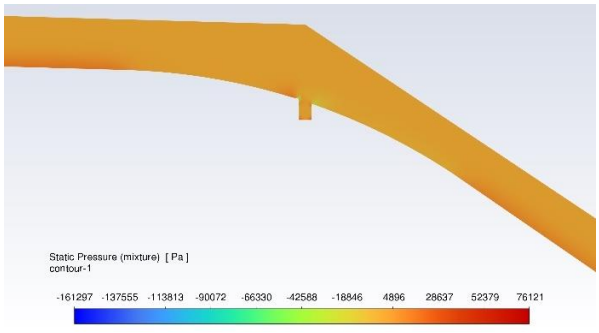

Series-A

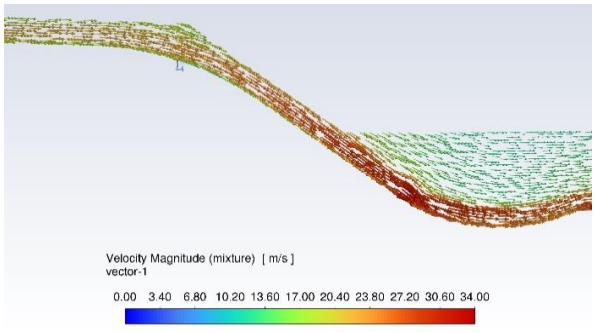

Series-A

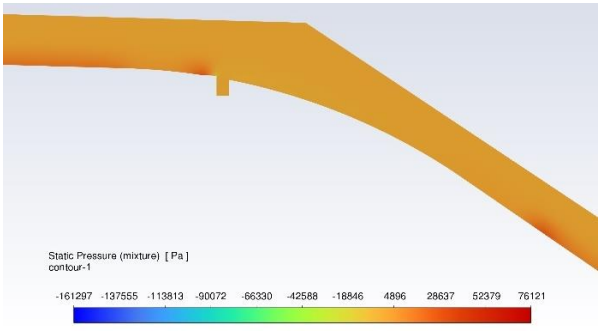

Series-B

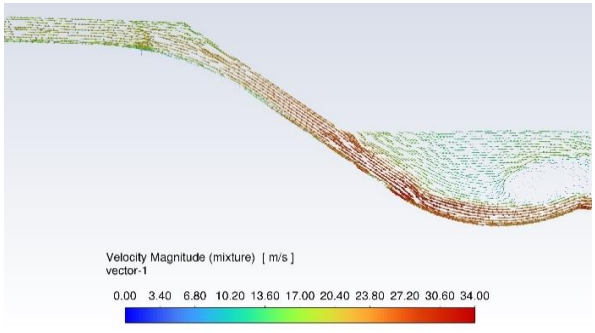

Series-B

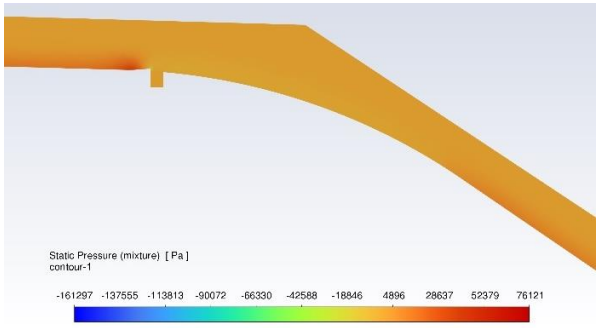

Series-C

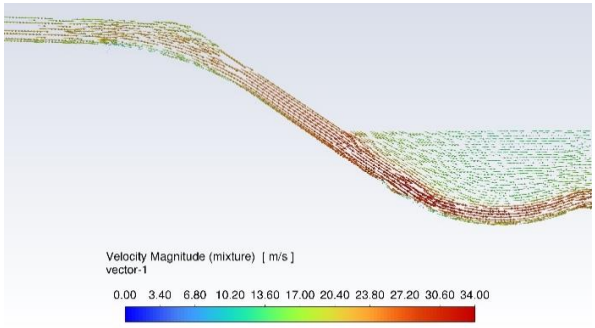

Series-C

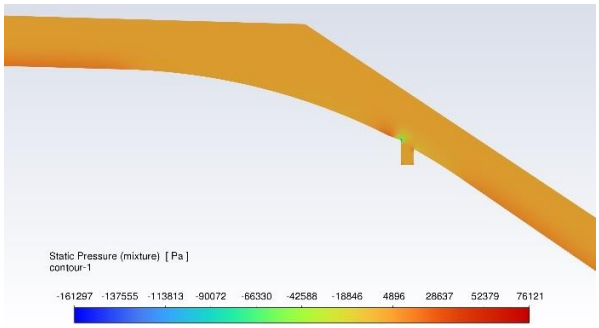

Series-D

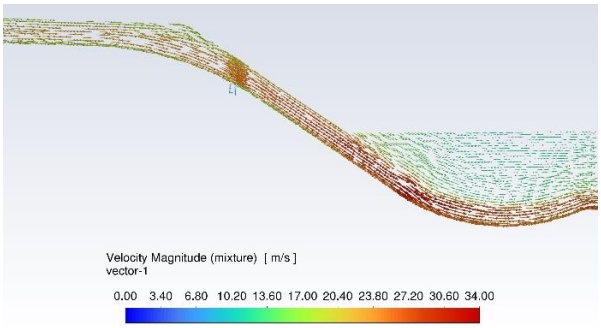

Series-D

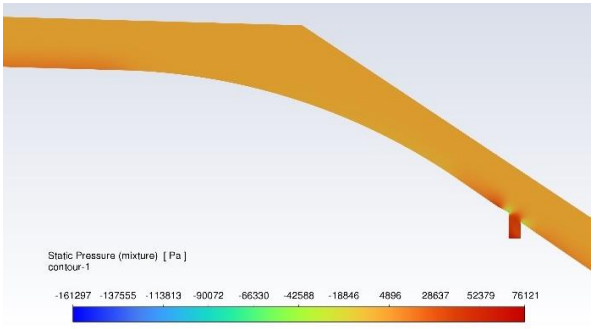

Series-E

(a) Contour of pressure

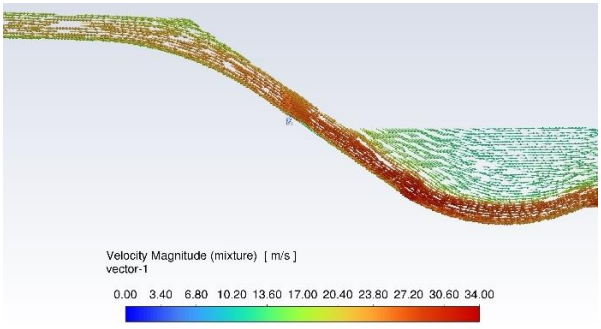

Series-E

(b) Vector of velocity

Figure 5. Pressure and Velocity at Chute-way Case of A – E

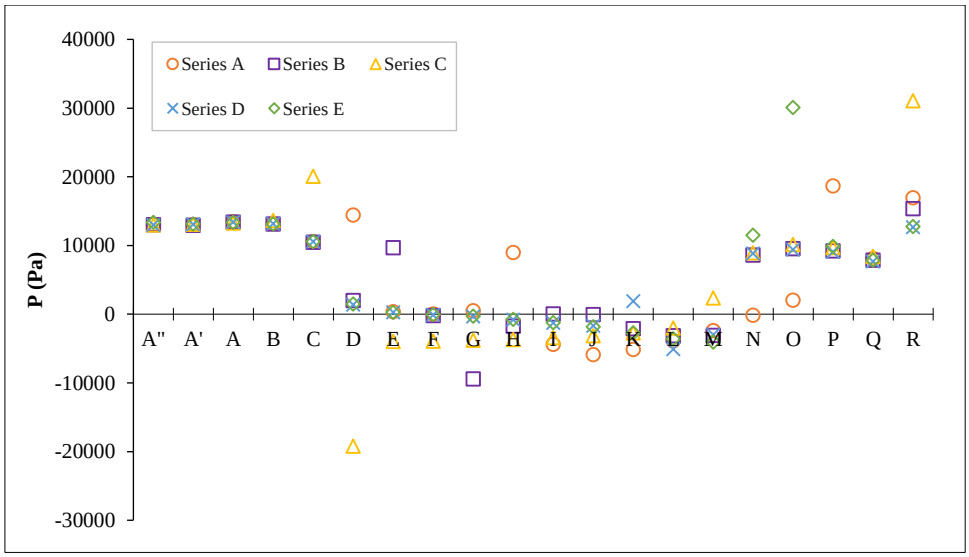

Figure 6. Measurement of Pressure at Chute-way Series of A – E

For Series A, pressure decreases from upstream positive values (≈13–14 kPa at A″–D) to a minimum of −5.92 kPa at point J, before gradually recovering downstream to 18.64 kPa at point P and 16.91 kPa at point R. The negative-

pressure region is confined primarily between points I–L, indicating a localized and controlled low-pressure zone. This behavior suggests that aeration occurs sufficiently upstream to stabilize the pressure gradient across the curvature. In Series B, the pressure drop is more severe and spatially broader. The minimum pressure reaches −9.45 kPa at point G, with negative values extending from F to M. Although downstream recovery occurs, pressures remain lower than those in Series A over a longer distance. This indicates reduced effectiveness in suppressing low-pressure development when the aerator is shifted downstream. Series C exhibits the most critical pressure response. Extremely low pressures are observed immediately downstream of the aerator, with a minimum of −19.24 kPa at point D, followed by sustained negative pressures up to point M. Although pressure recovers further downstream, this configuration produces the largest pressure fluctuation amplitude, indicating unstable jet re-attachment and a high cavitation susceptibility near the curvature.

In contrast, Series D and E show comparatively milder minimum pressures (−5.11 kPa at point L for Series D and −4.08 kPa at point M for Series E). However, the negative-pressure zones in these configurations shift downstream and expand, occurring mainly beyond the curvature. This indicates that aeration is introduced too late to effectively protect the most critical region near the slope transition. Overall, the pressure analysis demonstrates that Series A provides the most favorable pressure distribution, characterized by moderate minimum pressure and limited spatial extent of negative-pressure zones. This finding is consistent with prior studies, which emphasize placing aerators just upstream of the expected minimum-pressure region to stabilize pressure gradients and reduce cavitation risk [3, 9, 25].

3.2.3. Distribution of Velocity

The velocity distribution along the chute further illustrates the hydraulic response to aerator placement. Figure 7 illustrates the velocity profiles for all configurations. As shown in Figure 6, upstream velocities are similar for all configurations, ranging from 19.1–19.6 m/s at points A″–C, reflecting identical inflow conditions. Differences become pronounced downstream of the aerator and across the curvature.

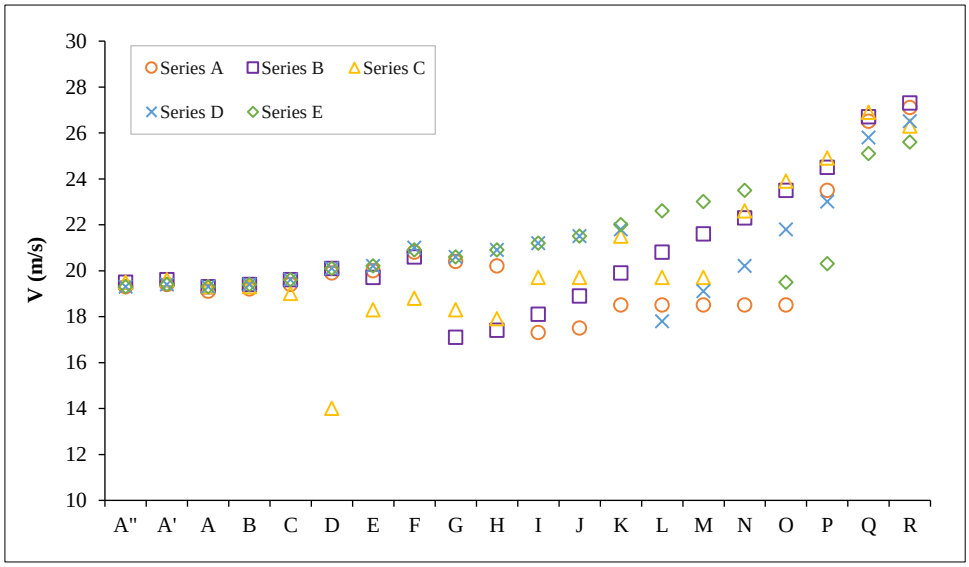

Figure 7. Measurement of Velocity at Chute-way Series of A–E

In Series A, velocity decreases moderately downstream of the deflector, from 20.0 m/s at point E to 17.3 m/s at point I, corresponding to the formation of a stable air cavity and partial jet separation. This localized deceleration is followed by a smooth velocity recovery, reaching 26.5–27.1 m/s at points Q–R. Such a gradual recovery indicates controlled re-attachment and reduced velocity gradients near the bed. For Series B, a stronger velocity reduction is observed in the cavity region, with velocities dropping to 17.1–17.4 m/s at points G–H. Although velocity increases downstream, the recovery gradient is steeper than in Series A, suggesting stronger jet oscillation and less stable re-attachment. Series C shows a similar but more pronounced pattern, with velocities decreasing to 14.0 m/s at point D and remaining below 19 m/s over several downstream points. This significant deceleration coincides with the extreme pressure drop observed in Series C and indicates excessive jet lifting and unstable cavity behavior.

In Series D and E, velocity reduction downstream of the aerator is minimal. Velocities remain relatively high (≈20–21 m/s) immediately after the deflector and increase rapidly downstream. This attached-flow regime limits jet separation and air cavity development, resulting in reduced velocity fluctuations but also diminished aeration effectiveness near the curvature. Comparatively, Series A achieves the most balanced velocity distribution, combining sufficient local deceleration to enable effective aeration with smooth downstream acceleration that avoids abrupt velocity gradients. Similar trends have been reported in previous experimental and numerical studies on deflector–groove and offset aerators, where controlled velocity reduction and gradual recovery were identified as key conditions for stable aeration and cavitation mitigation [8, 14, 20].

3.3. Air Mass and Characteristic of Cavitation

The aeration performance of each configuration was evaluated based on the entrained air mass flow rate through the air ducts and its effectiveness in improving the cavitation index along the chute bed. Among the five configurations, Series D exhibits the highest air mass entrainment (66.9 kg/s), followed by Series A (63.0 kg/s), Series C (55.8 kg/s), Series B (29.3 kg/s), while Series E shows negligible air intake, indicating a fully flooded groove. These results confirm that air supply alone does not directly govern cavitation mitigation effectiveness.

Although Series D provides the highest air mass inflow, its pressure and cavitation index distributions reveal relatively strong spatial fluctuations downstream of the deflector. Local oscillations near the deflector lip indicate an unstable aeration pattern, in which a large portion of the injected air is rapidly dissipated and does not form a continuous air cushion along the bed. In contrast, Series A demonstrates a more uniform pressure recovery and a smoother cavitation index profile, indicating that entrained air is more effectively distributed beneath the main flow layer.

The spatial distribution of the cavitation index σ for all configurations is shown in Figure 8, while the corresponding values at measurement points A″–R are summarized in Table 5. Overall, Series A consistently maintains higher σ-values over most of the chute length, particularly across the critical downstream region (points K–R), where σ remains above approximately 0.40. In comparison, Series D and Series E exhibit lower σ-values, with extended zones where σ approaches 0.30–0.35, indicating a higher cavitation risk. Notably, the minimum σ-values for Series A are confined to the far downstream region, where flow velocity is already stabilized and concrete exposure is less critical.

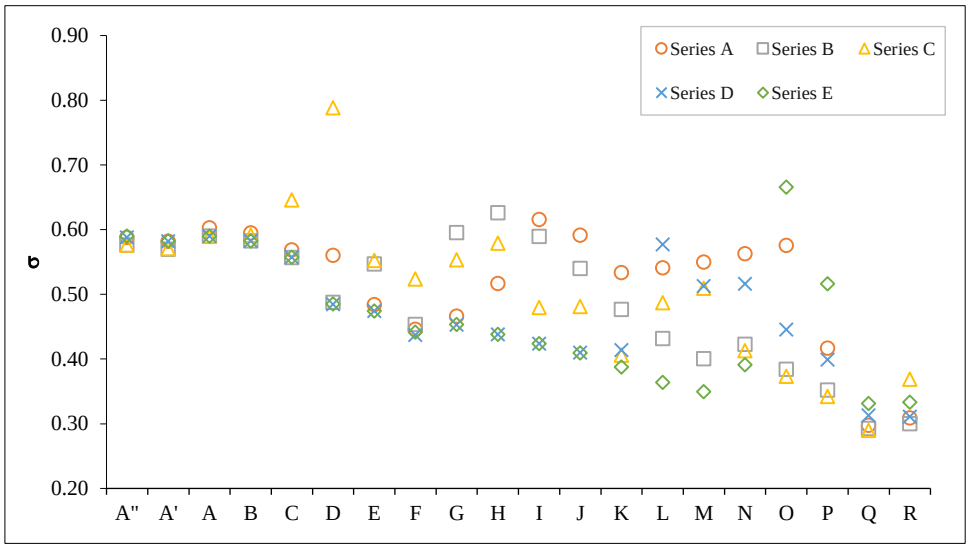

Figure 8. Cavitation index (σ) distribution along the spillway chute for aerator configurations Series A–E at Q = 1,154.3 m³/s

Table 5. Cavitation Index at Observation Points for Various Aerator Locations

Point	2A	2B	2C	2D	2E
19.3	0.60	0.58	0.58	0.60	0.60
19.4	0.59	0.58	0.58	0.59	0.59
19.3	0.61	0.60	0.60	0.60	0.60
19.4	0.60	0.59	0.60	0.59	0.59
19.6	0.58	0.56	0.65	0.56	0.56
20.1	0.57	0.49	0.80	0.49	0.49
20.2	0.49	0.55	0.56	0.48	0.48
20.9	0.45	0.46	0.53	0.44	0.45
20.6	0.47	0.60	0.56	0.46	0.46
20.9	0.52	0.63	0.59	0.44	0.44
21.2	0.62	0.60	0.49	0.43	0.43
21.5	0.61	0.55	0.49	0.42	0.42
22	0.54	0.48	0.39	0.42	0.39
22.6	0.55	0.44	0.49	0.59	0.37
23	0.56	0.41	0.52	0.52	0.35
23.5	0.57	0.43	0.42	0.52	0.40
19.5	0.58	0.39	0.38	0.45	0.67
20.3	0.42	0.36	0.35	0.40	0.52
25.1	0.30	0.30	0.29	0.32	0.34
25.6	0.31	0.30	0.37	0.31	0.34

The results also show that configurations with upstream aerator placement (Series A–C) shift the lowest σ-values away from the concave vertical curve, thereby reducing the spatial extent of cavitation-prone zones. Conversely, downstream placement (Series D–E) allows negative pressures to fully develop at the curvature before aeration becomes effective. This behavior confirms that aerator location relative to the pressure-minimum zone is more influential than the magnitude of air supply, consistent with established aeration theory for high-velocity spillway flows.

Regarding numerical uncertainty, variations in σ are primarily driven by local pressure predictions, which are sensitive to turbulence modeling and jet–bed interaction. The SST k–ω model captures adverse pressure gradients and flow re-attachment more reliably than standard k–ε models, yet some local deviations in σ (±5–10%) are unavoidable near the deflector lip and curvature transition. However, the relative ranking of aerator configurations remains robust, and the spatial trends in σ are consistent across the entire chute.

In summary, Series A provides the most effective balance between air entrainment, pressure stabilization, and cavitation risk reduction, despite not delivering the maximum air mass flow rate. These findings demonstrate that optimal aerator performance on multi-slope spillways is achieved through strategic placement within the pressure-transition zone rather than by maximizing air supply alone. Comparable conclusions were reported by Pfister & Chanson [3], Wu et al. [10], and Liu et al. [15], who emphasized that aerator location relative to the pressure field is more critical than maximizing air discharge alone.

3.4. Efficiency of Aeration and Optimization of Aerator Position

The aeration efficiency of a chute aerator should be assessed not solely by the magnitude of supplied air, but by its effectiveness in mitigating cavitation along the spillway bed. Table 6 summarizes the key performance indicators for the five aerator configurations, including entrained air mass flow rate ($\dot{m}_{air}$), minimum cavitation index (σ_{min}), its location, and the spatial extent of the cavitation risk zone defined as $\sigma < 0.4$. Although Series D delivers the highest air intake ($\dot{m}_{air}$ = 66.9 kg/s), its cavitation mitigation performance is limited by a relatively long risk zone (11.8 m) and the occurrence of σ_{min} at the downstream end (point R). In contrast, Series A provides a more favorable balance, maintaining a high air intake ($\dot{m}_{air}$ = 63 kg/s) while confining the cavitation-prone zone to the shortest extent (5.8 m) and localizing σ_{min} at a single downstream point (Q, σ_{min} = 0.298). Series B and C exhibit the longest $\sigma < 0.4$ zones (15.5 m), despite moderate to high air entrainment, indicating that increased air supply alone does not ensure effective cavitation control. Series E shows negligible air intake and multiple separated risk zones, reflecting ineffective aeration due to unfavorable aerator placement.

Table 6. Summary of aeration performance and cavitation risk indicators for different aerator configurations

Series	m_{air} (kg/s)	σ_{min}	Location of σ_{min}	Cavitation risk zone length of $\sigma < 0.4$ (m)
A	63	0.298	Q	5.8
B	29.3	0.293	Q	15.5
C	55.8	0.290	Q	15.5
D	66.9	0. 311	R	11.8
E	0.01	0.331	Q	10.3 ; 6

The spatial distribution of cavitation index further highlights that the extent of the $\sigma < 0.4$ zone is a more reliable indicator of aeration effectiveness than air discharge alone. Consistent with previous studies on chute aerators and cavitation mitigation, optimal performance is achieved when the aerator is positioned within the pressure-transition region associated with curvature and slope change, enabling stable pressure recovery and limiting the downstream propagation of low-σ zones [5, 8-9, 11, 20, 23].

Therefore, Series A is identified as the optimal aerator configuration for the Tigadihaji multi-slope spillway, as it achieves the most efficient compromise between air entrainment capacity and cavitation-risk reduction, providing a practical and hydraulically robust solution for high-velocity spillways with concave vertical curvature.

4. Conclusion

This study numerically investigated the performance of a deflector–groove aerator installed on a high-velocity spillway with a concave vertical curvature under a design discharge of Q_{1000} = 1,154.3 m³/s, focusing on the influence of aerator location on flow characteristics, air entrainment, and cavitation mitigation. The results demonstrate that aerator placement plays a decisive role in controlling flow separation, pressure recovery, and the formation of air cavities within the curvature region. Among the tested configurations, the aerator located near the center of the concave curvature (Series A) produced the most stable flow pattern, characterized by a continuous near-bed air layer and reduced pressure fluctuations compared with downstream placements.

Although Series D yielded the highest air mass intake (66.9 kg/s), it exhibited pronounced local pressure oscillations and an extended cavitation risk zone, indicating uneven aeration efficiency. In contrast, Series A achieved a favorable balance between air entrainment ($\dot{m}_{air}$ = 63 kg/s) and pressure stabilization, resulting in the shortest cavitation-prone zone ($\sigma < 0.4$) and a more uniform distribution of cavitation index along the chute. These findings confirm that effective cavitation mitigation depends not only on the quantity of entrained air but also on the spatial alignment of the aerator with the pressure-transition region induced by slope change and curvature.

Based on the combined assessment of pressure distribution, cavitation index, and aeration efficiency, Series A is identified as the optimal aerator configuration for the investigated multi-slope spillway. This outcome reinforces established aeration principles reported in previous studies, emphasizing that the balance between aerator location, local pressure conditions, and air-layer stability is fundamental to cavitation control in high-energy spillway flows. Future work should extend the present approach by examining variations in deflector and groove geometry and by exploring multi-aerator or offset-deflector configurations to enhance downstream protection while maintaining hydraulic efficiency.

5. Declarations

5.1. Author Contributions

Conceptualization, M.L.G. and P.T.J.; methodology, M.L.G. and V.D.; validation, M.L.G.; formal analysis, M.L.G.; investigation, M.L.G. and D.S.; resources, M.L.G. and L.M.L.; data curation, M.L.G. and D.S.; writing—original draft preparation, M.L.G. and P.T.J.; writing—review and editing, L.M.L. and V.D.; visualization, M.L.G. and D.S. All authors have read and agreed to the published version of the manuscript.

5.2. Data Availability Statement

The data presented in this study are available in the article.

5.3. Funding

The authors received no financial support for the research, authorship, and/or publication of this article.

5.4. Conflicts of Interest

The authors declare no conflict of interest.

6. References

[1] Boes, R. M., & Hager, W. H. (2003). Two-Phase Flow Characteristics of Stepped Spillways. Journal of Hydraulic Engineering, 129(9), 661–670. doi:10.1061/(asce)0733-9429(2003)129:9(661).

[2] Felder, S., & Chanson, H. (2011). Air-water flow properties in step cavity down a stepped chute. International Journal of Multiphase Flow, 37(7), 732–745. doi:10.1016/j.ijmultiphaseflow.2011.02.009.

[3] Pfister, M., & Chanson, H. (2014). Two-phase air-water flows: Scale effects in physical modeling. Journal of Hydrodynamics, 26(2), 291–298. doi:10.1016/S1001-6058(14)60032-9.

[4] Salehi, S., Mahmudi Moghadam, A., & Soori, S. (2023). Effect of the pipe bend of the morning glory spillway on the cavitation number. Flow Measurement and Instrumentation, 92, 102375. doi:10.1016/j.flowmeasinst.2023.102375.

[5] Gaskin, S. J., Aubel, T., & Holder, G. (2003). Air demand for a ramp-offset aerator as a function of spillway slope, ramp angle and Froude number. Proceedings of the 30th IAHR World Congress, 24–29 August 2003, Thessaloniki, Greece.

[6] Aydin, M. C. (2017). Aeration efficiency of bottom-inlet aerators for spillways. ISH Journal of Hydraulic Engineering, 24(3), 330–336. doi:10.1080/09715010.2017.1381576.

[7] Wang, Y., Deng, J., & Wei, W. (2022). Investigation on the Cavity Backwater of Chute Aerators under Various Atmospheric Pressures. Water (Switzerland), 14(9), 1513. doi:10.3390/w14091513.

[8] Wu, J. H., Ma, F., & Dai, H. C. (2011). Influence of filling water on air concentration. Journal of Hydrodynamics, 23(5), 601–606. doi:10.1016/S1001-6058(10)60155-2.

[9] Ma, F., & Wu, J. H. (2012). Flow regimes below aerators for discharge tunnels. Journal of Hydrodynamics, 24(3), 378–382. doi:10.1016/S1001-6058(11)60258-8.

[10] Wu, J. H., Li, D., Ma, F., & Qian, S. T. (2013). Fin characteristics of aerator devices with lateral deflectors. Journal of Hydrodynamics, 25(2), 258–263. doi:10.1016/S1001-6058(13)60361-3.

[11] Qian, S. T., Wu, J. H., Ma, F., Xu, J. R., Peng, Y., & Wang, Z. (2014). Cavity filling water control below aerator devices. Journal of Hydrodynamics, 26(3), 424–430. doi:10.1016/S1001-6058(14)60048-2.

[12] Wei, W., Deng, J., & Zhang, F. (2016). Development of self-aeration process for supercritical chute flows. International Journal of Multiphase Flow, 79, 172–180. doi:10.1016/j.ijmultiphaseflow.2015.11.003.

[13] Bai, R., Liu, S., Wang, W., & Zhang, F. (2019). Experimental investigation of the dissipation rate in a chute aerator flow. Experimental Thermal and Fluid Science, 101, 201–208. doi:10.1016/j.expthermflusci.2018.10.015.

[14] Liu, X., Bai, R., Wang, H., & Liu, S. (2022). Flow aeration by an offset aerator: Air entrainment, bubbly flow turbulence, and adaptive-window cross-correlation processing. Experimental Thermal and Fluid Science, 132, 110572. doi:10.1016/j.expthermflusci.2021.110572.

[15] Liu, X., Bai, R., & Liu, S. (2023). Air entrainment scale effects in chute aerator flows. European Journal of Mechanics, B/Fluids, 99, 163–172. doi:10.1016/j.euromechflu.2023.01.005.

[16] Ye, F., Xu, W., & Wei, W. (2022). Experimental study of the air concentration diffusion in aerated chute flows downstream of lateral and bottom aerators. AIP Advances, 12(2), 0077783. doi:10.1063/5.0077783.

[17] Su, P.-l., Liao, H.-s., Qiu, Y., & Li, C.-j. (2009). Experimental Study on a New Type of Aerator in Spillway with Low Froude Number and Mild Slope Flow. Journal of Hydrodynamics, 21(3), 415–422. doi:10.1016/s1001-6058(08)60165-1.

[18] Yang, J., Teng, P., & Lin, C. (2019). Air-vent layouts and water-air flow behaviors of a wide spillway aerator. Theoretical and Applied Mechanics Letters, 9(2), 130–143. doi:10.1016/j.taml.2019.02.009.

[19] Li, S., Yang, J., & Liu, W. (2021). Estimation of aerator air demand by an embedded multi-gene genetic programming. Journal of Hydroinformatics, 23(5), 1000–1013. doi:10.2166/hydro.2021.037.

[20] Aydin, M. C., Isik, E., & Ulu, A. E. (2020). Numerical modeling of spillway aerators in high-head dams. Applied Water Science, 10(1). doi:10.1007/s13201-019-1126-2.

[21] Bagherzadeh, S., Ghaeini-Hessaroeyeh, M., & Fadaei-Kermani, E. (2025). Prediction of cavitation damage using SVM model based on air–water two-phase flow over dam spillway. Applied Water Science, 15(4), 70. doi:10.1007/s13201-025-02406-4.

[22] Dong, Y., Li, G., Liu, S., Li, S., Li, P., & Wei, Y. (2024). A Study on the Shape of Parabolic Aeration Facilities with Local Steepness in Slow Slope Chutes. Water (Switzerland), 16(11), 1574. doi:10.3390/w16111574.

[23] Ali, S. A., Khan, N. M., Sarwar, M. K., Zaffar, M. W., Tariq, A. U. R., Ullah, U., & Abbas, Y. (2024). Hydraulic investigation of flows at high-head overflow spillway with multiple aerators: a physical and numerical study of Mohmand Dam, Pakistan. Aqua Water Infrastructure, Ecosystems and Society, 73(8), 1725–1740. doi:10.2166/aqua.2024.180.

[24] Safiloo, F., Salmasi, F., Arvanaghi, H., Abbaspour, A., & Abraham, J. (2025). Investigating flow characteristics in different types of chute spillway aerators. ISH Journal of Hydraulic Engineering, 31(4), 686–706. doi:10.1080/09715010.2025.2515486.

[25] Kalateh, F., & Aminvash, E. (2025). Numerical investigation of aerator position effects on two-phase flow and hydraulic efficiency in morning glory spillway. Innovative Infrastructure Solutions, 10(1), 10. doi:10.1007/s41062-024-01812-y.

[26] Wang, Y., Wei, W., Song, T., & Deng, J. (2025). Air Entrainment of Chute Aerators Under Different Atmospheric Pressures. Water (Switzerland), 17(18), 2734. doi:10.3390/w17182734.

[27] PUPR. (2022). Final report on the physical model of the Tigadihaji Dam. Balai Hidrolika dan Geotektik Keairan, Kementerian Pekerjaan Umum dan Perumahan Rakyat (PUPR), Jakarta, Indonesia. (In Indonesian).

[28] Falvey, H. T. (1990). Cavitation in chutes and spillways. Bureau of Reclamation, US Department of the Interior, Denver, United States.